Evaluation of new spin foam vertex amplitudes with boundary states

Igor Khavkine

July 16, 2022

Abstract

The numerical evaluation algorithms for the new spin foam vertex amplitudes proposed by Engle, Pereira & Rovelli and Freidel & Krasnov, recently developed by the author, are extended to efficiently include a large class of boundary states (factored states). A concrete pragmatic proposal is made for a semi-classical state, encompassing to both the Barrett-Crane and new models. Two computations using this boundary state are described together with a uniform comparison methodology for the three different models: semi-classical wave packet propagation and graviton 2-point function evaluation. The new algorithms are applied to the wave packet propagation problem, indicating that the Magliaro, Rovelli and Perini's hypothesis of good semiclassical behavior of the new models may not hold under more general conditions (with unfrozen j-spins).

PACS numbers: 04.60.Pp

1 Introduction

Spin foam models are an attempt to produce a theory of quantum gravity starting from a discrete, path integral-like approach. For the last decade, the standard spin foam model has been the one due to Barrett and Crane [9]. More recently, some shortcomings of the Barrett-Crane (BC) model have been identified [3, 4] and alternative models were proposed. Two leading alternatives are the Engle-Pereira-Rovelli (EPR) model (also referred to as the "flipped" vertex model) [16, 17] and the Freidel-Krasnov (FK) model [15, 18]. Here, as in much of the spin foam literature, we only discuss gravity in Riemannian signature.

Having been defined, the new models must be tested to see whether their semiclassical behavior is an improvement over the BC model. So far, two test problems have been proposed: semiclassical wave packet propagation [23], and evaluation of the graviton 2-point function [10, 14, 25]. Both problems require the computation of large sums, where the spin foam vertex amplitude is contracted with a suitably defined boundary state. These computations, while important for extracting the physical content of the new spin foam models, have so far not been tractable.

In a previous paper [20], the author has described an efficient numerical algorithm, based on the existing Christensen-Egan (CE) algorithm for the BC model, to evaluate the new spin foam vertex amplitudes. This algorithm was used to examine their asymptotic behavior. The present paper extends this algorithm to allow efficient

contraction of the vertex amplitude with a large class of boundary states (so-called *factored* boundary states).

Application of this algorithm to the wave packet propagation problem shows that, under fairly general conditions, the shape of the propagated wave packet does not agree with the expected semiclassical result, unlike hypothesized in [23].

Section 2 reviews the two proposed calculations that require the introduction of boundary states. Also, the class of factored boundary states is defined. Section 3 describes the appropriate CE algorithm generalizations. Section 4 shows the results of applying the algorithms of section 3 to the problems of section 2. Finally, section 5 concludes with a discussion of the results and future work.

2 Spin foams with boundary states

Spin foam models in general are described in [5, 6] and especially from a computational perspective in [7, 8, 20, 21]. Briefly, a spin foam model of gravity starts with a triangulated 4-manifold (possibly with boundary). Its *dual 2-complex* consists of cells dual to simplices of the triangulation: a *dual vertex* for each 4-simplex, a *dual edge* for each tetrahedron, and a *dual face* for each triangle. A labelling of the dual 2-complex by *spins* constitutes a *spin foam*. The labelling of the dual 2-complex depends on the model, but at a minimum includes an integer label for each dual face, called a *spin*[1]. Besides specifying this labelling, a *spin foam model* also assigns an amplitude to a given spin foam. This amplitude for a spin foam F takes the form

$$A(F) = \prod_f A_f(F) \prod_e A_e(F) \prod_v A_v(F), \tag{1}$$

where f, e, and v range respectively over dual faces, dual edges, and dual vertices. Each of the amplitudes $A_f(F)$, $A_e(F)$, $A_v(F)$ may depend on its own label and on the labels of adjacent dual cells.

The BC model assigns integer labels only to dual faces (*j-spins*). The EPR model also assigns integer labels to dual edges (*i-spins*). The FK model additionally assigns integers to each dual edge-dual face pair (*k-spins*)[2].

The partition function for a spin foam model is defined to be

$$Z = \sum_F A(F), \tag{2}$$

where the summation ranges over all spin foams F. The expectation value of an observable O is calculated according to the formula

$$\langle O \rangle = \frac{1}{Z} \sum_F O(F) A(F). \tag{3}$$

If the underlying triangulated manifold is closed, then corresponding spin foams are also said to be *closed*. Similarly, if the underlying manifold has a boundary, the

[1] Most of the time these integers identify representations of $SU(2)$, hence the name *spin*. Technically, they are *twice-spins*, since they do not take on half-integral values

[2] It should be noted that the current paper uses integral twice-spins to label $SU(2)$ irreps, following [19], while the original references for the EPR [16] and FK [18] models use half-integral spins. However, the i and j labels of [16] coincide numerically with the current notation, while the l, j and k labels of [18] coincide respectively with i, $j/2$, and k in current notation.

spin foams are said to be *open* and also have a boundary. Any open spin foam F_O can be decomposed into $F_O = F \cup F_B$, where F_B labels only cells dual to the boundary, while F labels only cells dual to triangulation simplices in the interior. For an open spin foam F_O, its amplitude may be naturally generalized to

$$A(F_O) = A(F, F_B)\Psi(F_B), \tag{4}$$

where the bulk amplitude $A(F, F_B)$ is the usual amplitude defined according to (1), and Ψ is referred to as the boundary state, which may be fixed separately from the bulk amplitude. The partition function and observables are then written as

$$Z_\Psi = \sum_{F,F_B} A(F, F_B)\Psi(F_B), \quad \text{and} \quad \langle O \rangle_\Psi = \frac{1}{Z_\Psi} \sum_{F,F_B} O(F, F_B)A(F, F_B)\Psi(F_B). \tag{5}$$

As an illustration, an open spin foam model with a boundary state may arise if we split a closed spin foam model in two parts and average over one of them. Suppose a close triangulated manifold can be decomposed into two bulk pieces and the codimension-1 boundary between them. Any closed spin foam F_C can then be decomposed as $F_C = F \cup F_B \cup F'$, where F_B corresponds to the boundary, F to the interior of the piece we are interested in and F' to the interior of the other piece. The partition function may be rewritten as follows:

$$\begin{aligned} Z &= \sum_{F_C} A(F, F_B)A(F_B)A(F', F_B) \\ &= \sum_{F,F_B} A(F, F_B)A(F_B) \sum_{F'} A(F', F_B) = \sum_{F,F_B} A(F, F_B)\Psi(F_B), \end{aligned} \tag{6}$$

where $\Psi(F_B)$ has been defined by averaging over all spin foams F'. This example is very similar to the separation of a large system into a subsystem and the environment in quantum statistical mechanics.

The simplest example of a triangulation with boundary is a single 4-simplex, with the five tetrahedra forming its boundary. The 2-complex dual to the interior consists of a single dual vertex, corresponding to the 4-simplex itself. The dual 2-complex of the boundary consists of five dual edges, dual to the tetrahedra, and of ten dual faces, dual to the triangular faces of the tetrahedra. The problems described in sections 2.1 and 2.2, have previously only been considered for a single 4-simplex. This paper restricts attention to the same case.

The algorithms that will be described in section 3 are applicable only to a restricted class of states, *factored* states. Such a state must factor in a specific way with respect to the spins it depends on. The various spin labels of the dual complex of the 4-simplex and the corresponding notation are summarized in figure 1, referred to as the *pent graph*. The vertices of the pent graph correspond to the five boundary tetrahedra of the 4-simplex, while the ten edges connecting them correspond to its triangles. This graph is labelled by 35 spins, i_e, $j_{c,e}$, and $k^x_{c,e}$. The e subscript numbers the vertices of the pent graph; it is always taken mod 5. The spin $j_{c,e}$ labels the graph edge joining vertices e and $e + c$. The superscript x stands for either p or q; $k^p_{c,e}$ labels the vertex-edge pair e and (c, e), while $k^q_{c,e}$ labels the pair $e + c$ and (c, e). Again, all vertex indices are taken mod 5.

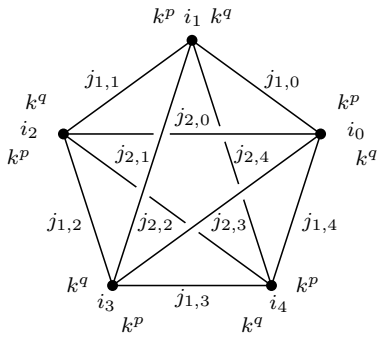

Figure 1: The *pent graph*, summarizing the indexing scheme for i-, j-, and k-spins.

The class of factored states is somewhat different for each model. However, it contains at least all of the following:

$$\Psi(F_B) = \prod_{c,e} \psi_{c,e}(j_{c,e}) \prod_{e} \psi_e(i_e) \prod_{x,f,e} \psi_{x,f,e}(k^x_{f,e}), \tag{7}$$

where the products range over all i-, j-, and k-spins. Spins not part of a particular model may be dropped from the product. The ψs are arbitrary functions with finite support. For each model, the class of factored states is enlarged, as factors of $\Psi(F_B)$ may be allowed to depend on specific clusters of spins, instead of only individual ones. The details will be elaborated in section 3.

Nearly all previous work on the problems described in sections 2.1 and 2.2 have been considered only for factored boundary states. While this class of states is restrictive, its limitations may be overcome. Note that the expectation value $\langle O \rangle_\Psi$ in equation (5) is equal to the ratio of two quantities that are both linear in the boundary state Ψ. The numerical algorithm computes this numerator and denominator separately. Since any boundary state Ψ can be approximated by linear combinations of factored states with finite support, so can $\langle O \rangle_\Psi$ be approximated for any boundary state Ψ.

2.1 Semiclassical wave packets

The problem presented in this section was introduced in [23]. Consider a single 4-simplex. As shown in the preceding section, it is described by a spin foam with a single dual vertex and i-, j-, and k-spins labelling cells dual to its boundary. An arbitrary functional $\Psi(F_B)$ depending on these boundary spins, in general, corresponds to a statistical quantum state, that is, a density matrix.

This is analogous to the single point particle, where an arbitrary density matrix $\rho(x_f, x_i) = \langle x_f, t_f | \rho | x_i, t_i \rangle$ can be described in terms of its matrix elements between eigenstates of the Heisenberg position operator at different times[3], $x(t_i)|x_i, t_i\rangle = x_i|x_i, t_i\rangle$ and $x(t_f)|x_f, t_f\rangle = x_f|x_f, t_f\rangle$. The density matrix is pure only if it can be factored, $\rho(x_f, x_i) = \psi(x_f, t_f)^* \psi(x_i, t_i)$, where $\psi(x, t)$ denotes the time evolution of a given wave function.

[3]In this representation, the functional $\rho(x_f, x_i)$ is not necessarily symmetric, $\rho(x_i, x_f) \neq \rho(x_f, x_i)^*$.

Similarly, we can split the boundary of the 4-simplex into two pieces[4], the initial $(-)$ and the final $(+)$. Then, for a pure boundary state, we should be able to write

$$\Psi(F_B) = \Psi_+(F_B^+)^* \Psi_-(F_B^-), \tag{8}$$

where $F_B^\pm$ respectively depend only on spins labelling the dual complex of the corresponding piece of the boundary.

The relationship of the two boundary state factors $\Psi_\pm(F_B^\pm)$ is constrained in two ways. On the one hand (in the limit of $\hbar \to 0$), the amplitude should be peaked on those geometries that correspond to the boundary of a classical 4-geometry satisfying Einstein's equations. On the other hand, Ψ_+ should be a time-evolved, "future" version of the "past" Ψ_-, which can be expressed as

$$\Psi_+(F_B^+) = \sum_{F, F_B^-} A(F, F_B) \Psi_-(F_B^-), \tag{9}$$

where the summation over the boundary spin foams keeps F_B^+ fixed and varies F_B^-.

Reference [23] has proposed an expression for $\Psi(F_B)$, in the context of the EPR model, which should reproduce a flat regular 4-simplex. This state has gaussian dependence on individual spins and hence is factorable in a convenient way. The problem is then to compute $\Psi_+(F_B^+)$ both from (8) and from (9), and to compare the two. Agreement is interpreted as evidence of a correct semiclassical limit for the EPR model.

A concrete expression for the proposed $\Psi(F_B)$ is

$$\Psi(F_B) = N \prod_{c,e} \psi_{c,e}(j_{c,e}) \prod_e \psi_e(i_e, \{j_{c,e}\}), \quad \text{with} \tag{10}$$

$$\psi_{c,e}(j_{c,e}) = e^{-\frac{1}{\tau}(j_{c,e} - j_0)^2 + i\Theta j_{c,e}}, \tag{11}$$

$$\psi_e(i_e, \{j_{c,e}\}) = \sqrt{\frac{2i_e + 1}{\theta(2i_e, 2j_{1,e}, 2j_{2,e})\theta(2i_e, 2j_{1,e-1}, 2j_{2,e-2})}} e^{-\frac{3}{4j_0}(i - i_0)^2 + i\frac{\pi}{2} i_e}, \tag{12}$$

where N is a normalization factor, j_0 determines the size of the regular 4-simplex and $\cos\Theta = -1/4$. The parameter τ controls the size of quantum fluctuations about the classical values of j.

The wave packet propagation geometry given in [23] fixes $\tau = 0$ in the state (11), freezing all j-spins to the background value j_0. Effectively, only the dependence of $\Psi(F_B)$ on the i-spins was considered. A single vertex of the 4-simplex is labelled as "past", while the remaining four as "future". The four "future" vertices form a tetrahedron, whose dual is labelled by an i-spin. This labelled dual edge constitutes F_B^+, while the remaining four dual edges labelled by i-spins constitute F_B^-. This propagation geometry will be referred to as *EPR 4-1 propagation*.

An immediate generalization, feasible with the algorithm described in section 3, is to relax the $\tau = 0$ limitation. The choice of τ should be consistent with the parameters used in the graviton propagator calculations. Thus, following[5] [14], we let the wave

[4]Technically speaking, this decomposition is unique only in Lorentzian signature. In Riemannian signature, different choices of the decomposition should correspond to different possible Wick rotations.

[5]It should be noted that reference [14] uses half-integral spins, while we use integral twice-spins to label $SU(2)$ irreps. A j label from Christensen, Livine and Speziale corresponds numerically to $j/2$ in current notation.

packet width depend on the background spin,

$$\tau = 4j_0/\alpha, \tag{13}$$

with α is a positive parameter.

It is important to note that the boundary state proposed above, in equation (10), is not the best possible candidate to generalize the calculations of [23]. Its major advantage is that it belongs to the class of factored states. In fact, a more realistic proposal for a boundary state where both i- and j-spins are allowed to vary was given by Rovelli and Speziale [26]. Unfortunately, Rovelli and Speziale's boundary state does not factor nicely and requires more sophisticated techniques to be used efficiently. As such, the boundary state proposed above should be seen more as a test of the algorithms presented in section 3 and an attempt to explore the qualitative effects of introducing j-dependent (and below k-dependent) boundary states.

Now, a uniform methodology should be constructed for each of the three models. As only j-spins are common among the models, we propose the following wave packet propagation geometry. One possibility is to propagate wave packets from nine of the j-spins to the remaining one. This configuration corresponds to fixing a single triangle (defined by three vertices of a 4-simplex) in the "future", while relegating the other nine triangles (containing at least one of the two remaining 4-simplex vertices) to the "past". Thus, the single j-labelled face dual to the "future" triangle will constitute F_B^+, while the rest of the boundary spin foam will constitute F_B^-, including all i- and k-spins, if any. This propagation geometry will be referred to as *9-1 propagation*.

Another alternative is to assign a vertex of the 4-simplex to the "future", together with the six triangles sharing sharing it. The remaining four triangles are relegated to the "past". Thus, F_B^+ consists of the six j-labelled faces dual to the "future" triangles, with the rest of the boundary spin foam constituting F_B^-. This propagation geometry will be referred to as *4-6 propagation*. There are numerous other possibilities. However, the two described above are sufficient to illustrate an application of the numerical algorithms and to show the qualitative behavior to be expected from propagated wave packets.

The boundary state (10) is valid only for the EPR model. For the BC model, we simply drop the ψ_e factors:

$$\Psi(F_B) = N \prod_{c,e} \psi_{c,e}(j_{c,e}). \tag{14}$$

And for the FK model we must add extra $\psi^x_{c,e}$ factors for each k-spin:

$$\Psi(F_B) = N \prod_{c,e} \psi_{c,e}(j_{c,e}) \prod_{e} \psi_e(i_e, \{j_{c,e}\}) \prod_{x,c,e} \psi^x_{c,e}(k^x_{c,e}, j_{c,e}). \tag{15}$$

Because the k-spins are closely geometrically associated with j-spins, we use the same gaussian state parameters:

$$\psi^x_{c,e}(k^x_{c,e}, j_{c,e}) = \sqrt{\frac{2k^x_{c,e}+1}{\theta(j_{c,e}, j_{c,e}, 2k^x_{c,e})} C_{j_{c,e}k^x_{c,e}}}\, e^{-\frac{\alpha}{4j_0}(k^x_{c,e}-j_0)^2 + i\Theta k^x_{c,e}}, \tag{16}$$

$$C_{jk} = \frac{(j+1)!}{(j-k)!}\frac{(j+1)!}{(j+k+1)!}. \tag{17}$$

The square root factor includes the FK model edge normalization, as does (12) for the EPR model.

2.2 Graviton propagator

The graviton propagator is well defined in the perturbative quantization of gravity. It is computed as the 2-point function $G_{\mu\nu\rho\sigma}(x,y) = \langle 0|h_{\mu\nu}(x)h_{\rho\sigma}(y)|0\rangle$, where $|0\rangle$ is the Minkowski vacuum, and $h_{\mu\nu}(x)$ is the metric perturbation. General relativity requires that, in harmonic gauge [27], the decay rate of the 2-point function, for large separation between points x and y, is the same as for the Newtonian force of gravitational attraction: inverse distance squared. The framework for computing the equivalent of the graviton propagator in the spin foam formalism was elaborated in [10, 22, 24, 25]. The quantum area spectrum is $A = \ell_P^2(j+1)$, with j a dual face spin foam label and ℓ_P the Plank length. Dimensional arguments then give the expected decay of the propagator as $O(1/j)$, with j being the typical size for the chosen spin foam boundary state.

The expected asymptotic behavior of the graviton propagator has been checked for the BC model both analytically and numerically [14, 22, 25]. Unfortunately, the expected behavior was only reproduced for certain tensor components of $G_{\mu\nu\rho\sigma}(x,y)$, but not for others [3, 4]. This negative result has prompted the introduction of EPR and FK spin foam models as alternatives to the BC model. The challenge is to compute the graviton propagator for the new models and check that it has the expected asymptotic behavior.

Following [14], we show the computational set up for the BC model and then extend it to other models. Consider again a single 4-simplex with boundary and the corresponding spin foam. We associate the area $A = \ell_P^2(j+1)$ to each triangle, depending on the j-spin labelling its dual. The goal is to compute the correlation between observables depending on the triangle areas [cf. (5)]:

$$W_{ce,c'e'} = \frac{1}{Z_\Psi} \sum_{F,F_B} A(F,F_B) h_{ce}(F_B) h_{c'e'}(F_B) \Psi(F_B), \tag{18}$$

where ce and $c'e'$ index the specific $j_{c,e}$ and $j_{c',e'}$ spins taking part in the correlation. Again following [14], the boundary state[6] is a semiclassical gaussian state peaked around a flat 4-simplex, whose scale is set by j_0:

$$\Psi(F_B) = \prod_{c,e} e^{-\frac{\alpha}{4j_0}(j_{c,e}-j_0)^2 + i\Theta j_{c,e}}, \tag{19}$$

where $\cos\Theta = -1/4$, and j_0 sets the scale for the background geometry, as in the previous section. The observables measure the fluctuation of areas squared:

$$h_{ce}(F_B) = \frac{(j_{c,e}+1)^2 - (j_0+1)^2}{(j_0+1)^2}. \tag{20}$$

Note that the product $\Psi'(F_B) = h_{ce}(F_B)\Psi(F_B)$ has exactly the same factorizability properties as $\Psi(F_B)$. This property allows both the numerator and denominator in (18) to be computed on the same footing.

Again, an important task here is the generalization of this calculation to the EPR and FK models. This generalization essentially requires the specification of a boundary state that describes a semiclassical state peaked around the flat regular 4-simplex.

[6] We incorporate the "measure" discussed in [14] into the boundary state and pick the trivial case $k = 0$.

Since this is the same requirement used in picking out the boundary states in the section on wave packet propagation, simply choose the same ones. That is, the BC, EPR and FK boundary states are specified, respectively, by equations (14), (10), and (15).

3 Numerical algorithms

We will start by reviewing the spin foam vertex evaluation algorithms with fixed boundary spins. The dual face and edge amplitudes, A_f and A_e, are trivial to compute. The difficulty lies in evaluating the dual vertex amplitude A_v, which is where we will concentrate. All algorithms described in this section are extensions of the original CE algorithm for the BC model [13] and all fall into the same product-trace pattern:

$$A_v(\{j_{c,e}, i_e, k^x_{c,e}\}) = (-)^S \sum_{m^-,m^+} \phi \,\mathrm{tr}[M_4 M_3 M_2 M_1 M_0], \tag{21}$$

where $(-)^S$ is an overall sign factor, ϕ depends only on $m^\pm$ and M_e are matrices of compatible dimensions, collectively depending on all the spins. Each of these elements may be specified separately in any incarnation of this algorithm. In all cases presented below, we have

$$\phi = (-)^{\frac{1}{2}(m^- - m^+)}(m^- + 1)(m^+ + 1). \tag{22}$$

However, the M_e matrices will be redefined for each variation of the algorithm. The notation for various boundary spins is summarized with the pent graph in figure 1.

The run time complexity of a generalized CE algorithm may be estimated as follows. Suppose that the spin arguments to A_v in (21) are of average magnitude j. Then, generally, the dimensions of the matrices M_e scale as a power of j; say, each matrix is $O(j^d) \times O(j^d)$, for some integer d. The run time will be dominated by filling the M_e matrices and by the product-trace operation.

The product-trace may be implemented as follows: each of the $O(j^d)$ standard basis vectors is subjected to matrix-vector multiplies by the M_e and appropriate elements of the result vectors are accumulated into the trace. If the M_e are dense, then the cost of a matrix-vector multiply is $O(j^{2d})$. However, we shall see below that this complexity may be reduced by decomposing each M_e into sparse factors. Hence, we will parametrize the matrix-vector multiply complexity as $O(j^D)$, with D no greater than $2d$, and the product-trace complexity as $O(j^{d+D})$.

The upper bound on the time needed to fill an $O(j^d)\times O(j^d)$ matrix M_e is $O(j^{2d+f})$, if each matrix element is computed in $O(j^f)$ time. Sparse factorization improves this estimate as well, which we will parametrize as $O(j^{F+f})$, where F does not exceed $2d$. In all cases we have examined, $d + D > F + f$, which implies that the product-trace operation dominates matrix filling in run time for large spins. More detailed discussions of possible optimizations for matrix filling can be found in [21] and [20]. Below, we will give the best known value of f for each algorithm.

Finally, the outer $m^\pm$ sums in (21) also span ranges of size $O(j)$. Therefore, the run time complexity of a generalized CE algorithm may be expressed as $O(j^{2+d+D})$.

The matrix elements of the M_e (computed in the following sections), will contain spin network evaluations that require certain inequality and parity constraints on their arguments. Solving these constraints yields precise matrix dimensions and bounds for any intermediate summations. The details are described in section 3.2 of [20]. It can

be shown that all matrix dimensions as well as intermediate summation bounds are finite. However, for that to be true in the presence of a boundary state, it is crucial that each factor of the boundary state (7) has finite support.

3.1 BC vertex

For the BC model, the vertex amplitude is only a function of the j-spins. As a slight abuse of notation, we will use the symbols i_e as indices (also referred to as spins, and directly analogous to the $i_e^{\pm}$ indices introduced for the other models) of the M_e matrices:

$$(M_e)_{i_e}^{i_{e+1}} = \frac{(i_e+1)\begin{bmatrix} i_e & j_{2,e} & m^- \\ i_{e+1} & j_{2,e-1} & j_{1,e}\end{bmatrix}\begin{bmatrix} i_e & j_{2,e} & m^+ \\ i_{e+1} & j_{2,e-1} & j_{1,e}\end{bmatrix}}{\theta(j_{2,e-1}, i_{e+1}, j_{1,e})\,\theta(j_{2,e}, i_e, j_{1,e})\,\theta(j_{2,e}, i_{e+1}, m^-)\,\theta(j_{2,e}, i_{e+1}, m^+)}. \quad (23)$$

The sign factor from (21) is given by $S = \sum_{c,e} j_{c,e}$. The ranges of the i_e and m spins are specified by triangle inequalities and parity constraints satisfied by various spins. For a detailed derivation and for notation, see the original reference [13], and also [21] and its Appendix[7].

The structure of the M_e matrices will become increasingly important and will grow in sophistication in the algorithms presented below. Hence, it is convenient to introduce a graphical notation to represent this structure. In this simplest case we have:

$$M_e = \ ^{i_{e+1}} \text{——} \boxed{M_e} \text{——} \ ^{i_e}. \quad (24)$$

Each strand represents an index. The incoming and outgoing strands correspond to the i_e and i_{e+1} indices of M_e and are labelled as such. The product-trace operation in (21) is effected by concatenating appropriately labelled strands. Further features of the notation will be elaborated as they are introduced.

Each matrix M_e is dense and of size $O(j) \times O(j)$. According to the discussion at the beginning of this section, we have $d = 1$, $D = 2$, $f = 0$, $F = 2$, and $2 + d + D = 5$. Hence, we recover the well known $O(j^5)$ run time complexity of the original CE algorithm.

3.2 New vertices

For the EPR model, the amplitude is a function of both i- and j-spins, while the FK model is also a function of k-spins. Here, we give the explicit FK formula, with the EPR version obtained by setting $k^x_{c,e} = j_{c,e}$. The matrix elements of M_e are

$$(M_e)_{i_e^- i_e^+}^{i_{e+1}^- i_{e+1}^+} = Q^{e+1}_{i_{e+1}^- i_{e+1}^+} (T^e_-)^{i_{e+1}^-}_{i_e^-} (T^e_+)^{i_{e+1}^+}_{i_e^+} \left[P^e_{i_e^- i_e^+} N^e_{i_e^-} N^e_{i_e^+} \frac{(-)^{\frac{1}{2}(i_e^- + i_e^+ - 2i_e)}}{\theta(i_e^-, i_e^+, 2i_e)} \right] \quad (25)$$

[7]Note however, that these references use half-integral spins, while the present paper uses integer twice-spins.

where

$$(T^e_\pm)^{i^\pm_{e+1}}_{i^\pm_e} = \frac{\begin{bmatrix} i^\pm_e & j_{1,e} & j_{2,e-1} \\ i^\pm_{e+1} & m^\pm & j_{2,e} \end{bmatrix}}{\theta(i^\pm_{e+1}, m^\pm, j_{2,e})}, \tag{26}$$

$$N_{i^\pm_e} = \frac{\Delta_{i^\pm_e}}{\theta(i^\pm_e, j_{1,e}, j_{2,e})\theta(i^\pm_e, j_{2,e-2}, j_{1,e-1})}, \tag{27}$$

$$P^e_{i^-_e\, i^+_e} = \sum_{n_p} (-)^{\frac{1}{2}(j_{1,e}+j_{2,e}-n_p)} \Delta_{n_p} \frac{\begin{bmatrix} 2k^p_{2,e} & 2k^p_{1,e} & n_p \\ i^-_e & i^+_e & 2i_e \end{bmatrix}}{\theta(n_p, j_{1,e}, j_{2,e})} \frac{\begin{bmatrix} j_{1,e} & j_{1,e} & j_{2,e} \\ i^-_e & n_p & 2k^p_{1,e} \end{bmatrix}}{\theta(i^-_e, n_p, 2k^p_{1,e})} \frac{\begin{bmatrix} j_{2,e} & j_{2,e} & j_{1,e} \\ i^+_e & n_p & 2k^p_{2,e} \end{bmatrix}}{\theta(i^+_e, n_p, 2k^p_{2,e})}, \tag{28}$$

and

$$Q^e_{i^-_e\, i^+_e} = \sum_{n_q} (-)^{\frac{1}{2}(j_{2,e-2}+j_{1,e-1}-n_q)} \Delta_{n_q} \frac{\begin{bmatrix} 2k^q_{1,e-1} & 2k^q_{2,e-2} & n_q \\ i^-_e & i^+_e & 2i_e \end{bmatrix}}{\theta(n_q, j_{2,e-2}, j_{1,e-1})} \frac{\begin{bmatrix} j_{2,e-2} & j_{2,e-2} & j_{1,e-1} \\ i^-_e & n_q & 2k^q_{2,e-2} \end{bmatrix}}{\theta(i^-_e, n_q, 2k^q_{2,e-2})} \frac{\begin{bmatrix} j_{1,e-1} & j_{1,e-1} & j_{2,e-2} \\ i^+_e & n_q & 2k^q_{1,e-1} \end{bmatrix}}{\theta(i^+_e, n_q, 2k^q_{1,e-1})}. \tag{29}$$

For a detailed derivation and for bounds on the various summations, see [20].

The matrix elements of M_e are indexed by the pairs (i^-_e, i^+_e) and (i^-_{e+1}, i^+_{e+1}). In graphical notation, M_e has the following structured factorization.

$M_e =$ 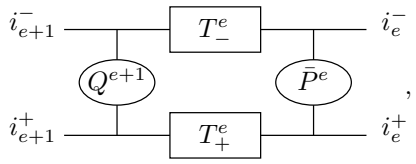

, (30)

where $\bar{P}^e$ stands for the entire bracketed term in (25). Unmarked vertices in the above diagram essentially correspond to Kronecker deltas. The notation is saying that both P^e and Q^{e+1} are diagonal matrices acting on the space of vectors indexed by (i^-_e, i^+_e) or (i^-_{e+1}, i^+_{e+1}). On the other hand, the $T^e_\pm$ matrices are block diagonal, acting separately on the $-$ and $+$ indices.

The dimension of each M_e is $O(j^2) \times O(j^2)$, implying $d = 2$. However, each M_e decomposes into sparse (diagonal or block diagonal) factors. The filling complexity parameters for the largest of these factors, $\bar{P}$ and Q, are $f = 1$, $F = 2$, and $F + f = 3$. Also, the cost of a matrix-vector multiply is parametrized by $D = 2 + 1 = 3$, giving $2 + d + D = 7$. Therefore, the run time complexity of evaluating an EPR or FK vertex amplitude is $O(j^7)$, as originally pointed out in [20]. This estimate compares favorably to simply treating M_e as a dense $O(j^2) \times O(j^2)$ matrix, which would imply an overall $O(j^8)$ run time complexity.

Contracting a boundary state, as described in section 2, with the vertex amplitude (21) gives the following partition function

$$Z_\Psi = \sum_{\{j_{c,e}, i_e, k^x_{c,e}\}} A_v(\{j_{c,e}, i_e, k^x_{c,e}\}) \Psi(\{j_{c,e}, i_e, k^x_{c,e}\}). \tag{31}$$

A naive approach to the problem of computing Z_Ψ would wrap an algorithm to compute A_v (as described so far in this section) in as many outer sums as there are spins in $\{j_{c,e}, i_e, k^x_{c,e}\}$. Namely, for the BC model, this would produce a calculation of run time complexity $O(j^{5+10}) = O(j^{15})$, with 10 outer spin sums. The EPR model would yield $O(j^{7+15}) = O(j^{22})$, with 15 outer spin sums, and the FK model $O(j^{7+35}) = O(j^{42})$, with 35 outer spin sums. Clearly, with the naive approach, these problems become intractable. Fortunately, when dealing with a factored state (as defined tentatively in section 2 and more precisely in the following sections), these summations may be absorbed into a redefinition of the M_e matrices, producing again a generalized CE algorithm:

$$Z_\Psi = \sum_{m^-,m^+} \phi \operatorname{tr}[M_4 M_3 M_2 M_1 M_0], \tag{32}$$

where ϕ is still defined by equation (22) and the sign factor is necessarily absorbed into the M_e. This approach is described in the next two sections.

It is important to note that the dimensions of the M_e matrices may be strongly impacted by the presence of a finitely supported boundary state. It is convenient for our purposes to keep the assumption that, even in the presence of a boundary state, the summation range for each spin is still of order $O(j)$. The run time complexity will be analyzed only for this case. However, the same analysis can be easily performed in other cases, where some of the spin summation ranges are significantly different.

3.3 BC vertex with boundary states

For the BC model, consider a factored boundary state of the form

$$\Psi(\{j_{c,e}\}) = \prod_{c,e} \psi_{c,e}(j_{c,e}). \tag{33}$$

The dependence of the matrices given in (23) on $\{j_{c,e}\}$ allows us to obtain the form (32) with the following redefinition:

$$(M_e)^{j_{2,e} i_{e+1}}_{j_{2,e-1} i_e} = \frac{(i_e+1)\,\psi_{2,e-1}(j_{2,e-1})}{\theta(j_{2,e}, i_{e+1}, m^-)\,\theta(j_{2,e}, i_{e+1}, m^+)} \sum_{j_{1,e}} \psi_{1,e}(j_{1,e}) \frac{\begin{bmatrix} i_e & j_{2,e} & m^- \\ i_{e+1} & j_{2,e-1} & j_{1,e} \end{bmatrix} \begin{bmatrix} i_e & j_{2,e} & m^+ \\ i_{e+1} & j_{2,e-1} & j_{1,e} \end{bmatrix}}{\theta(j_{2,e-1}, i_{e+1}, j_{1,e})\,\theta(j_{2,e}, i_e, j_{1,e})}. \tag{34}$$

Graphically, we represent the above equation as

$M_e =$ 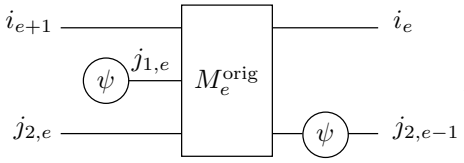

, (35)

where M_e^{orig} corresponds to the right hand side of equation (23) and ψ refer to the appropriate factors of the boundary state (33). The tadpole ψ shows an internal summation over $j_{1,e}$ necessary to form the matrix elements of M_e. It is shown here to highlight the location of the extra summation insertion and the possible relation of

$\psi_{1,e}$ to other spins. Note that, without any modification to the evaluation algorithm, we can generalize the notion of factored boundary states to include factors of the form $\psi(j_{1,e}, j_{2,e}, j_{2,e-1})$.

Notice that in this case M_e is dense and of size $O(j^2) \times O(j^2)$. Hence, the algorithm's runtime complexity is $O(j^8)$, as $d = 2$, $D = 2 + 2$, and $2 + d + D = 8$, while the filling parameters are $f = 1$ and $F = 4$. Interestingly enough, the *tets*[8] satisfy an identity which allows us to decompose M_e into sparse factors speeding up both the product-trace and matrix filling, thus reducing the run time complexity to $O(j^7)$. This identity is known as the Biedenharn-Elliot identity [11, 19]:

$$\frac{\begin{bmatrix} A & B & C \\ a & b & c \end{bmatrix} \begin{bmatrix} A' & B' & C' \\ a & b & c \end{bmatrix}}{\theta(a,b,c)} = \sum_s \Delta_s \frac{\begin{bmatrix} s & C' & B' \\ a & B & C \end{bmatrix}}{\theta(s,A,A')} \frac{\begin{bmatrix} s & A' & C' \\ b & C & A \end{bmatrix}}{\theta(s,B,B')} \frac{\begin{bmatrix} s & B' & A' \\ c & A & B \end{bmatrix}}{\theta(s,C,C')}. \quad (36)$$

The product of two tets in equation (34) can be rewritten using this identity as

$$\begin{aligned} &\frac{\begin{bmatrix} i_e & j_{2,e} & m^- \\ i_{e+1} & j_{2,e-1} & j_{1,e} \end{bmatrix} \begin{bmatrix} i_e & j_{2,e} & m^+ \\ i_{e+1} & j_{2,e-1} & j_{1,e} \end{bmatrix}}{\theta(j_{2,e-1}, i_{e+1}, j_{1,e})} \\ &\qquad = \sum_{s_e} \Delta_{s_e} \frac{\begin{bmatrix} s_e & m^+ & j_{2,e} \\ i_{e+1} & j_{2,e} & m^- \end{bmatrix}}{\theta(s_e, i_e, i_e)} \frac{\begin{bmatrix} s_e & i_e & m^+ \\ j_{2,e-1} & m^- & i_e \end{bmatrix}}{\theta(s_e, j_{2,e}, j_{2,e})} \frac{\begin{bmatrix} s_e & j_{2,e} & i_e \\ j_{1,e} & i_e & j_{2,e} \end{bmatrix}}{\theta(s_e, m^-, m^+)}. \end{aligned} \quad (37)$$

Hence, we can factor M_e as follows:

$$\begin{aligned} (M_e)^{j_{2,e} i_{e+1}}_{j_{2,e-1} i_e} = \frac{(i_e+1)\,\psi_{2,e-1}(j_{2,e-1})}{\theta(j_{2,e}, i_{e+1}, m^-)\,\theta(j_{2,e}, i_{e+1}, m^+)} \sum_{s_e, j_{1,e}} \frac{\psi_{1,e}(j_{1,e}) \Delta_{s_e}}{\theta(j_{2,e}, i_e, j_{1,e})} \\ \frac{\begin{bmatrix} s_e & m^+ & j_{2,e} \\ i_{e+1} & j_{2,e} & m^- \end{bmatrix}}{\theta(s_e, i_e, i_e)} \frac{\begin{bmatrix} s_e & i_e & m^+ \\ j_{2,e-1} & m^- & i_e \end{bmatrix}}{\theta(s_e, j_{2,e}, j_{2,e})} \frac{\begin{bmatrix} s_e & j_{2,e} & i_e \\ j_{1,e} & i_e & j_{2,e} \end{bmatrix}}{\theta(s_e, m^-, m^+)}. \end{aligned} \quad (38)$$

Graphically, this rewriting can be show to be a factorization:

$M_e =$ 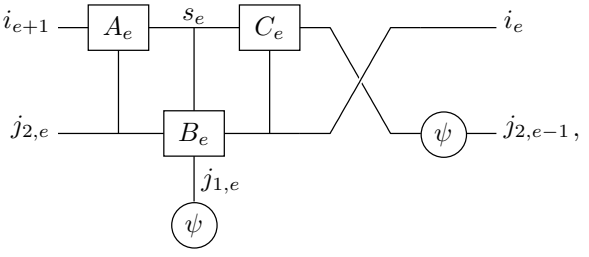

(39)

[8] The *tets* are the 2×3 arrays in square brackets, also called *tetrahedral networks*.

where the factors are given explicitly by

$$(A_e^{j_{2,e}})_{s_e}^{i_{e+1}} = \frac{\begin{bmatrix} s_e & m^+ & j_{2,e} \\ i_{e+1} & j_{2,e} & m^- \end{bmatrix}}{\theta(j_{2,e}, i_{e+1}, m^-)\,\theta(j_{2,e}, i_{e+1}, m^+)}, \tag{40}$$

$$(\psi{-}B_e^{s_e})_{i_e}^{j_{2,e}} = \sum_{j_{1,e}} \frac{\psi_{1,e}(j_{1,e})\Delta_{s_e}}{\theta(j_{2,e}, i_e, j_{1,e})} \frac{\begin{bmatrix} s_e & j_{2,e} & i_e \\ j_{1,e} & i_e & j_{2,e} \end{bmatrix}}{\theta(s_e, j_{2,e}, j_{2,e})}, \tag{41}$$

$$(C_e^{i_e})_{j_{2,e-1}}^{s_e} = (i_e+1)\frac{\begin{bmatrix} s_e & i_e & m^+ \\ j_{2,e-1} & m^- & i_e \end{bmatrix}}{\theta(s_e, i_e, i_e)\,\theta(s_e, m^-, m^+)}. \tag{42}$$

The decomposition is not completely unique; some of the terms may be distributed differently among the factors. However, in this factorization, the dependence of $\psi_{1,e}$ can only be generalized to $(j_{1,e}, j_{2,e})$.

Thus M_e is clearly decomposed into sparse factors, as each of A_e, B_e and C_e is dense in some indices, but diagonal in others. Computing the run time complexity, we get $O(j^7)$, as $d = 2$, $D = 2 + 1$, and $2 + d + D = 7$, while $f = 0$, $F = 3$ and $F + f = 3$ for filling either A or C. Note that the matrices B_e contracted with the $\psi_{1,e}$ factors do not depend on $m^\pm$. Hence, their computation can be done outside the $m^\pm$ summation loops and becomes completely subdominant.

Curiously, the most practically efficient implementation of the algorithm described in this section, as carried out by Christensen [12], turns out to be a hybrid of $O(j^8)$ and $O(j^7)$ versions. The factorization (39) greatly speeds up the matrix filling step, while the simplicity of the dense version of the product-trace operation is still advantageous for all inputs tried to date (up to $j_0 = 10$).

3.4 New vertices with boundary states

For the EPR and FK models, consider respectively

$$\Psi(\{j_{c,e}, i_e\}) = \prod_{c,e} \psi_{c,e}(j_{c,e}) \prod_{i_e} \psi_e(i_e) \tag{43}$$

and

$$\Psi(\{j_{c,e}, i_e, k^x_{c,e}\}) = \prod_{c,e} \psi_{c,e}(j_{c,e}) \prod_{i_e} \psi_e(i_e) \prod_{c,e} \psi_{x,c,e}(k^x_{c,e}). \tag{44}$$

Again, we shall only discuss the FK model explicitly, as the EPR model can be directly obtained by dropping k-dependent ψs and substituting $k = j$ everywhere else.

Essentially, we want to compute the quantity Z_Ψ from equation (31) with a suitably factorable boundary state Ψ and the vertex amplitude specified by equation (25). This expression for Z_Ψ can be cast into the form (32) with the following redefinition of M_e,

given directly in graphical form:

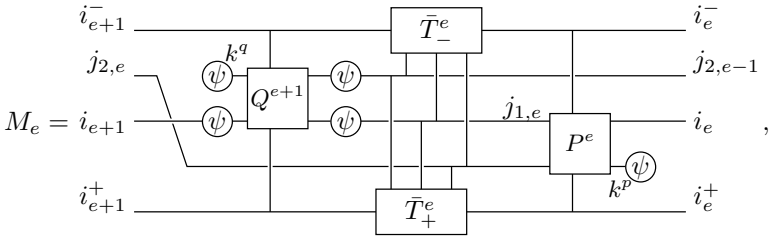

(45)

where $\bar{T}$ denotes a product of T and N from equations (26) and (27). Writing out this factorization of M_e with all indices shown explicitly, while straight forward, is cumbersome and not particularly enlightening. It should now be clear that, for this factorization of the M_e, individual factors of the boundary state may depend on clusters of spins of the form $(i_e, j_{1,e}, j_{2,e}, k^p_{1,e}, k^p_{2,e})$ as well as $(i_{e+1}, j_{1,e}, j_{2,e-1}, k^q_{1,e}, k^q_{2,e-1})$, which are compatible with possible factorizations of the boundary states proposed in sections 2.1 and 2.2.

Each M_e is of size $O(j^4) \times O(j^4)$, hence $d = 4$. However, because of the sparseness of the $\bar{T}$, P, and Q factors, each matrix-vector multiply takes $O(j^6)$ operations, since $D = 4 + 2$ for P and Q multiplies and, equivalently in terms of complexity, $D = 5 + 1$ for each $\bar{T}$ multiply. These numbers are identical for both EPR and FK models. On the other hand, filling the P and Q matrices for the EPR model does not involve summations over k-spins. Thus, the EPR filling complexity is parametrized by $f = 1$, $F = 5$, and $F + f = 6$, while the FK filling complexity is parametrized by $f = 3$, $F = 5$, and $F + f = 8$. The overall runtime complexity of the algorithm is $O(j^{12})$, $2 + d + D = 12$, both for the EPR and FK models. By conventional standards, this algorithm has a very high polynomial complexity exponent. However, it is still a substantial improvement over the naive $O(j^{22})$ or $O(j^{42})$ estimates found earlier.

4 Applications of the algorithms

The algorithms described in the preceding sections have already been implemented and applied in several contexts. Alesci, Bianchi, Magliaro and Perini [1] have used one variation to extend the original wave packet propagation calculations of [23], both to larger input spins and to different kinds of observables (although still keeping the j-spins frozen). Also, a highly optimized version of the algorithm presented in section 3.3 has been implemented by Christensen [12] and used to extract next-to-leading-order asymptotics information from the BC graviton propagator (cf. section 2.2), as a follow-up to [14]. While the method used in [14] is capable of handling higher input spins, the advantage of the new algorithm is much greater precision, which is better suited for subdominant asymptotics analysis.

Here, we apply the new algorithms to the problem of wave packet propagation described in section 2.1. We have already established that the boundary states proposed in that section are factored states compatible with the new algorithms. However, being gaussian, they do not have finite support. Fortunately, strong gaussian decay allows us to impose a finite cutoff while maintaining acceptable precision. The cutoff chosen for all computations presented below was 2.8 standard deviations about the mean. As a consequence, the range of each spin sum involved in the computation is still of order $O(j)$, as assumed by our run time complexity estimates.

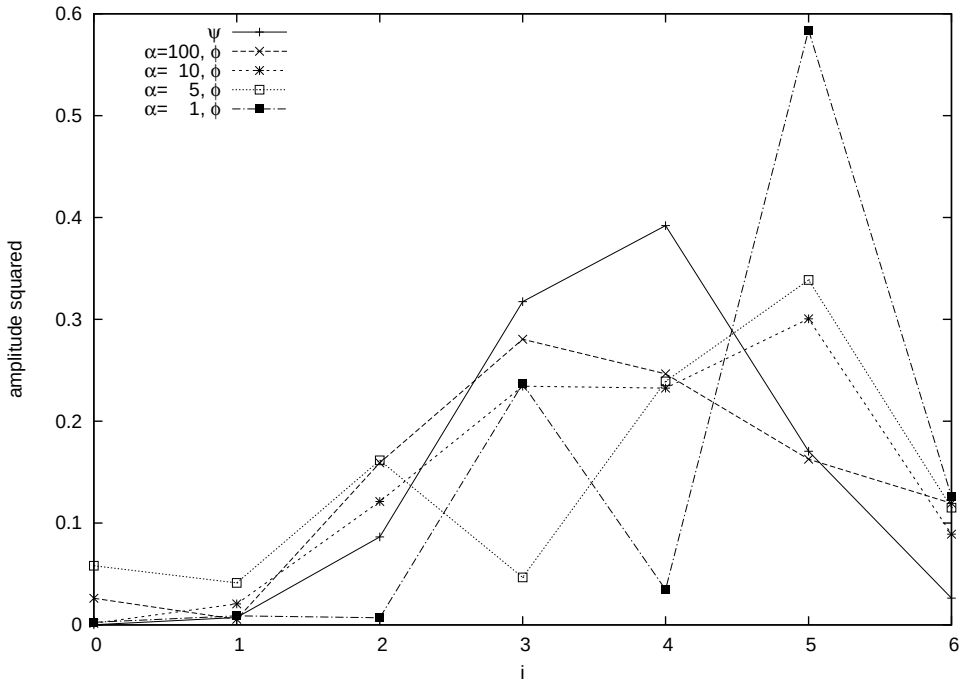

Figure 2: EPR 4-1 propagated (ϕ) and reference (ψ) wave packets, with $j_0 = 3$.

First, we can show the effect of introducing a non-zero τ in (11) and comparing with the calculations of [23], which kept $\tau = 0$, freezing all j-spins at the background value j_0. According to equation (13), the size of τ is inversely proportional to the parameter α. Figure 2 compares the reference wave packet ψ [cf. (12)] with several propagated wave packets ϕ (each with a different value of α) depending on the single fixed i-spin. The wave packets have been normalized such that their absolute values squared sum to 1. The wave packet with the largest value of α is essentially identical to the one obtained with all j-spins frozen at j_0. In that case, as shown previously in [23], the reference state ψ resembles the propagated wave packet in shape and mean. Unfortunately, as the width of the gaussian factors associated to j-spins increases (α decreases), the propagated wave packet quickly departs from ψ in both shape and mean. Notably, the mean shifts to a significantly higher value of i.

Second, we can compare the wave packets propagated by the three different models in the 9-1 geometry. Figure 3 shows the reference wave packets ψ [cf. (11)] and propagated wave packets ϕ, depending on the fixed j-spin and for two choices of α. These wave packets are also normalized. The BC wave packets appear to be pathological. They are completely dominated by zero spin. The EPR and FK wave packets do have a peak-like shape, however the mean and width of these peaks differ significantly from each other and the reference gaussian state.

Lastly, we compare the wave packets propagated by the three different models in the 4-6 geometry. In general, the propagated wave packet will depend on the four fixed j-spins. Unfortunately, it is impractical to either compute or display functions

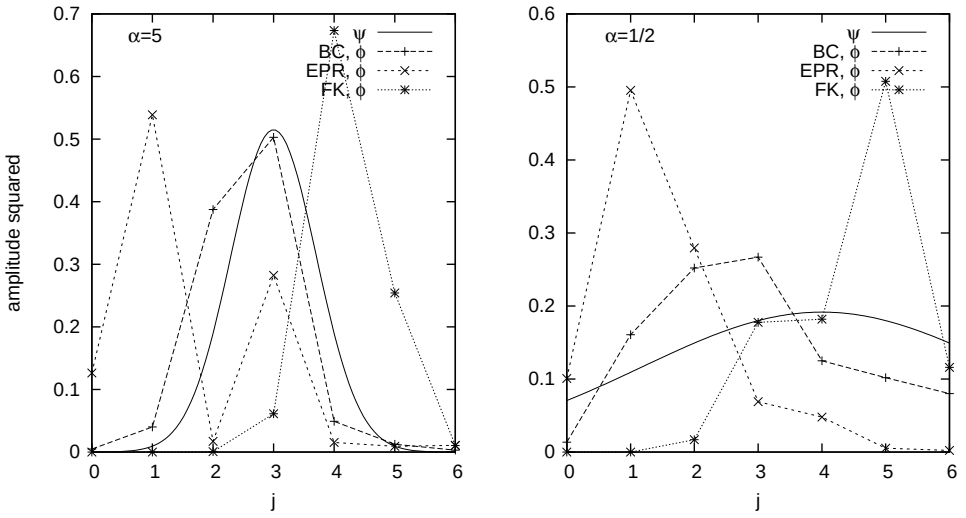

Figure 3: 9-1 propagated and reference wave packets for different models, with $j_0 = 3$.

on a 4-dimensional domain. Thus, all calculations have been done with the four fixed j-spins set equal. Figure 4 shows the reference wave packet ψ [cf. (11)] and propagated wave packets ϕ, depending on the common value of the fixed j-spins for two choices of α. These wave packets are again normalized. As is clearly seen from the figure, the propagated wave packets have in general very little similarity with the reference one. More pathological behavior is observed in the FK and BC models, the latter at $\alpha = 1/2$, since none of these curves resemble a well formed gaussian wave packet. In all cases, the propagated wave packet has little in common with the reference one.

5 Conclusion and Outlook

We have discussed open spin foam models with boundary states. Two prominent examples fitting into this framework that have appeared in the literature are the problems of semiclassical wave packet propagation (in the context of the EPR model) and computation of the graviton propagator matrix elements (in the context of the BC model). In section 2, we have extended both problems to each of the BC, EPR, and FK models. At the same time, we have proposed a uniform methodology for comparing results among the three models, despite their different spin argument structures. Although the boundary state proposed in section 2 is not ideal (see [26] for a more realistic proposal), it has the advantage of belonging to the class of factored states, allowing efficient numerical computation with algorithms of section 3. Moreover, the proposed state can still be used to gauge the qualitative behavior of unfreezing the j-spins.

A family of efficient numerical algorithms, capable of attacking these problems, has been constructed and implemented. The run time complexity of these algorithms has been analyzed and shown to be orders of magnitude superior to more naive approaches. Reference [23] had put forward the hypothesis that semiclassical wave packets, propa-

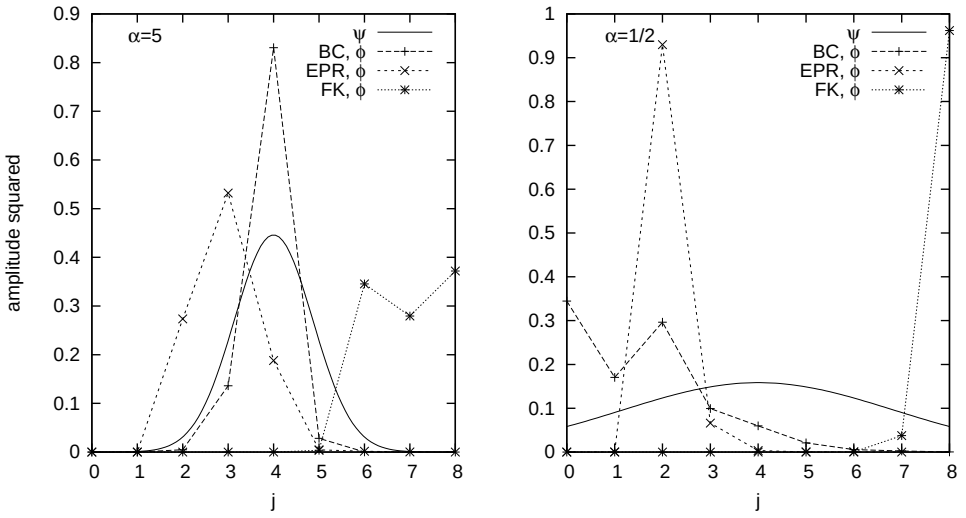

Figure 4: 4-6 propagated and reference wave packets for different models, with $j_0 = 4$.

gated using the EPR dual vertex amplitude, approximate a certain reference gaussian shape, which was demonstrated under somewhat restrictive conditions. An application of the numerical algorithms described above allowed a broader investigation of this question. The results indicate that this hypothesis may not hold under more general conditions, neither for the EPR nor for the other models (keeping in mind the caveat regarding the choice of boundary state).

These algorithms have also already been implemented and applied by other authors, as discussed in section 4. While, several wave packet propagation geometries have been examined, there are many other ones. Important questions remain: Is any one of them theoretically preferable to the others? What is the impact of directly using the unfactorable boundary state of [26]. Another immediate possibility for further investigation is the computation of the graviton propagator matrix elements in the EPR and FK models.

Acknowledgments

The author would like to thank Dan Christensen for suggesting this project. Also, Wade Cherrington, Carlo Rovelli, Elena Magliaro, Claudio Perini, Simone Speziale and Laurent Freidel have contributed through helpful discussions. The author was supported by an Ontario Graduate Scholarship and a SHARCNET Fellowship. Computational resources for this project were provided by SHARCNET.

References

[1] Alesci E, Bianchi E, Magliaro E, and Perini C 2008 Intertwiners dynamics in the flipped vertex (*Preprint* `arXiv:0808.1971`)

[2] Alesci E, Bianchi E, Magliaro E, and Perini C 2008 Asymptotics of LQG fusion coefficients (*Preprint* arXiv:0809.3718)

[3] Alesci E and Rovelli C 2007 Complete LQG propagator: Difficulties with the Barrett-Crane vertex *Physical Review D* **76** 104012–104033 (*Preprint* arXiv:0708.0883)

[4] Alesci E and Rovelli C 2008 Complete LQG propagator. II. Asymptotic behavior of the vertex *Physical Review D* **77** 044024–044034 (*Preprint* arXiv:0711.1284)

[5] Baez J C 1998 Spin foam models *Classical and Quantum Gravity* **15** 1827–58 (*Preprint* arXiv:gr-qc/9709052)

[6] Baez J C 2000 An introduction to spin foam models of quantum gravity and BF theory *Lecture Notes in Physics* **543** 25–94 (*Preprint* arXiv:gr-qc/9904025)

[7] Baez J C, Christensen J D, and Egan G 2002 Asymptotics of $10j$ symbols *Classical and Quantum Gravity* **19** 6489–513 (*Preprint* arXiv:gr-qc/0208010)

[8] Baez J C, Christensen J D, Halford T R, and Tsang D C 2002 Spin foam models of Riemannian quantum gravity *Classical and Quantum Gravity* **19** 4627–48 (*Preprint* arXiv:gr-qc/0202017)

[9] Barrett J W and Crane L 1998 Relativistic spin networks and quantum gravity *Journal of Mathematical Physics* **39** 3296–302 (*Preprint* arXiv:gr-qc/9709028)

[10] Bianchi E, Modesto L, Rovelli C, and Speziale S 2006 Graviton propagator in loop quantum gravity *Classical and Quantum Gravity* **23** 6989–7028 (*Preprint* arXiv:gr-qc/0604044)

[11] Carter J S, Flath D E, and Saito M 1995 The classical and quantum $6j$-symbols (*Mathematical Notes* vol 43) (Princeton, NJ: Princeton University Press)

[12] Christensen J D *Private communication.*

[13] Christensen J D and Egan G 2002 An efficient algorithm for the Riemannian $10j$ symbols *Classical and Quantum Gravity* **19** 1184–93 (*Preprint* arXiv:gr-qc/0110045)

[14] Christensen J D, Livine E R, and Speziale S 2007 Numerical evidence of regularized correlations in spin foam gravity (*Preprint* arXiv:0710.0617)

[15] Conrady F and Freidel L 2008 Path integral representation of spin foam models of 4d gravity (*Preprint* arXiv:0806.4640)

[16] Engle J, Pereira R, and Rovelli C 2007 The loop-quantum-gravity vertex-amplitude *Physical Review Letters* **99** 161301–161304 (*Preprint* arXiv:0705.2388)

[17] Engle J, Pereira R, and Rovelli C 2008 Flipped spinfoam vertex and loop gravity *Nuclear Physics B* **798** 251–290 (*Preprint* arXiv:0705.1236)

[18] Freidel L and Krasnov K 2008 A new spin foam model for 4d gravity *Classical and Quantum Gravity* **25** 125018–125053 (*Preprint* arXiv:0708.1595)

[19] Kauffman L H and Lins S L 1994 Temperley-Lieb recoupling theory and invariants of 3-manifolds (*Annals of Mathematics Studies* vol 134) (Princeton, NJ: Princeton University Press)

[20] Khavkine I 2008 Evaluation of new spin foam vertex amplitudes To appear.

[21] Khavkine I and Christensen J D 2007 q-deformed spin foam models of quantum gravity *Classical and Quantum Gravity* **24** 3271–3290 (*Preprint* arXiv:0704.0278)

[22] Livine E R and Speziale S 2006 Group integral techniques for the spinfoam graviton propagator *Journal of High Energy Physics* **11** 092–114 (*Preprint* arXiv:gr-qc/0608131)

[23] Magliaro E, Perini C, and Rovelli C 2007 Numerical indications on the semiclassical limit of the flipped vertex (*Preprint* arXiv:0710.5034)

[24] Modesto L and Rovelli C 2005 Particle scattering in loop quantum gravity *Physical Review Letters* **95** 191301–191304

[25] Rovelli C 2006 Graviton propagator from background-independent quantum gravity *Physical Review Letters* **97** 151301–151304 (*Preprint* arXiv:gr-qc/0508124)

[26] Rovelli C and Speziale S 2006 A semiclassical tetrahedron *Classical and Quantum Gravity* **23** 5861–5870 (*Preprint* arXiv:gr-qc/0606074)

[27] Wald R M 1984 General Relativity (Chicago, IL: University of Chicago Press)